Available online at www.sciencedirect.com
SCIENCE DIRECT®
Journal of Nuclear Materials 336 (2005) 233–242
journal of nuclear materials
www.elsevier.com/locate/jnucmat

# Thermodynamics of an empirical potential description of Fe–Cu alloys

A. Caro [a,*], P.E.A. Turchi [a], M. Caro [b], E.M. Lopasso [b]

[a] *Lawrence Livermore National Laboratory, P.O. Box 808, Livermore, CA 94551, USA*
[b] *Centro Atómico Bariloche, 8400 Bariloche, Argentina*

Received 18 May 2004; accepted 22 September 2004

**Abstract**

We apply molecular dynamics simulations based on a classic many-body potential to calculate the thermodynamic properties of Fe–Cu alloys. In a recent publication [E.M. Lopasso, M. Caro, A. Caro, P.E.A. Turchi, Phys. Rev. B 68 (2003) 214205], we report on computational thermodynamics tools applied to the prediction of the phase diagram of such a system. In this work, we calculate all its thermodynamic functions and cast the results in a so-called CALPHAD (Computer Coupling of Phase Diagrams and Thermochemistry, www.calphad.org) format to critically compare them with measured and calculated values as described in the CALPHAD database. From this comparison, conclusions are drawn on the power and limitations of empirical potentials to describe the thermodynamics of complex systems.


*PACS:* 81.30.Bx; 82.60.Lf; 02.70.Ns; 65.40.−b; 64.75.+g; 82.20.Wt

## 1. Introduction

The ability to perform atomistic computer simulations with predictive power in alloys is a subject that has attracted the attention of the simulator's community for a while. When mechanical properties and microstructure are the focus of attention, simulations have to be simple enough to allow dealing with a large number of atoms thus capturing the length scale that is relevant for this class of problems. The classic, empirical total energy expressions that are used have limitations to address real materials. In particular Fe alloys, the most commonly used material for structural applications, continue to be a major challenge for classic descriptions, as Fe is a complex element whose properties are determined by a subtle electronic behavior. Impurities and intrinsic defects in Fe play a significant role in determining its macroscopic mechanical properties, as is the case in nuclear reactor pressure vessels that undergo embrittlement as a consequence of radiation damage. Copper, an impurity present in commercial steels in a saturated solid solution phase, precipitates as a consequence of the microstructure damage generated by energetic neutrons. These precipitates, which act as obstacles for dislocation motion, are one of the most significant contributions to the increase of the ductile–brittle transition temperature that, in turns, determines the lifetime of the nuclear component. Therefore, understanding the precipitation process and the evolution of the precipitate structure is an important step in the description of steel aging in a radiation environment.

* Corresponding author.
*E-mail address:* caro2@llnl.gov (A. Caro).

0022-3115/$ - see front matter 
doi:10.1016/j.jnucmat.2004.09.018

Empirical simulations using classic potentials have a long history addressing this material. In 1990 Phythian et al. [1,2] reported a MD simulation that supported the first direct experimental evidence that the small Cu precipitates (2 nm) have bcc structure. They used interatomic potentials for pure Cu derived in 1987 by Ackland et al. [3]. In 1995, Osetsky et al. published a series of papers on the Fe–Cu system [4–6]. In 1997 Odette et al. reported Lattice-MC (LMC) simulations for complex Cu–Mn–Ni–Si structures in Fe [7]. They report parameters of a lattice embedded atom model Fe–Cu potential used in LMC cascade aging simulations. In 1999, Wirth and Odette [8] and Domain et al. [9] performed kinetic-LMC simulations of Fe–Cu alloys. These simulations confirm the presence of high vacancy concentrations in the precipitates. In 2001, Blackstock and Ackland, reported computer simulations of the phase transition of Cu precipitates in Fe–Cu alloys from the bcc structure to the twinned 9R crystal structure [10]. They used the interatomic potentials for Fe–Cu derived in 1997 by Ackland et al. [11].

Besides the work referenced here, there exists a body of research on ab initio techniques for this system that we shall not address in this work which focus on empirical potentials.

The problem of microstructure evolution of ferritic steels under irradiation involves complex thermodynamics of non-equilibrium and kinetic processes in alloys. Even though the many-body potentials have extensively been used to get insight into complex processes in several types of simple solids, in particular transition metals and some of their alloys [12,13], limited effort was devoted to the calculation of the complete equilibrium phase diagram predicted by this type of approximation and, from there, of the driving forces that govern non-equilibrium processes.

But Fe–Cu is just one example among the systems for which it would be useful to have a description based on a simple total energy expression from which forces can be derived, because then multi-million atom scale molecular dynamics or Monte Carlo computer simulations could be used to quantitatively predict the evolution of complex microstructures.

In a recent paper we reported on phase diagram calculations for Fe–Cu based on an classic Finnis–Sinclair (FS) description of the energetics [14]. The resulting phase diagram shows unexpected differences with the known assessed one [15]. FS-Fe shows a transition to an fcc phase right below melting that has no relation to the experimental one which is driven by magnetism. The melting point of FS-Fe (in the fcc phase) is at 2395 K, i.e., at 4/3 of the experimental $T_m$. FS-Cu has a transition to a bcc phase at 1147 K, i.e., at about 3/4 of $T_m$, which does not appear in real Cu; its melting point, in the bcc phase, is at 1582 K or 1.14 of the experimental $T_m$. The intermediate temperature region of the FS alloy shows an eutectoid at $x_{Cu} = 0.91$ and $T = 1025$ K and a peritectic at $x_{Cu} = 0.005$ at 2384 K, and a segregating bcc solid solution system with a low mixing energy, producing a miscibility gap that closes in the solid phase at a maximum of 1574 K, contrary to experiment. As a consequence of this artificial feature, there is a region around 1600 K of complete solid solubility in the bcc phase.

In this paper we reformulate the way thermodynamic quantities are represented as functions of temperature and concentration, following the Redlich–Kister expansion, which allows as performing a direct quantitative analysis of the differences between the model predictions and the assessed data for this system. As source of the assessed data for this system, we use the CALPHAD database (Computer Coupling of Phase Diagrams and Thermochemistry, www.calphad. org).

The paper is organized as follows: In Section 2 we briefly recall the CALPHAD [16,17] formalism. In Section 3, we clearly show the link between the numerical procedure used in our previous paper [14], and CALPHAD to conveniently describe all thermodynamic functions in alloys, and be able to compare our results from computational thermodynamics with those from standard databases in use with CALPHAD. In Section 4, we analyze in detail the sources of the discrepancies, namely, enthalpy, entropy, and free energy of each phase involved for the pure elements Fe and Cu, and the solid solutions of Fe–Cu, between the FS and the CALPHAD description of alloy thermodynamics. Finally, in Section 5, we draw some conclusions about the ability of empirical formalisms such as FS to account for realistic thermodynamic behavior as well as about the procedures that could be further explored to improve the agreement with experiment.

## 2. The CALPHAD thermodynamic modeling

The CALPHAD approach [16–18] represents a standardized way to express the thermodynamic information of a system in terms of the free energies of the phases of pure components, and the excess free energies of the mixtures. Once the free energies are expressed in this way, form suggested by the Scientific Group Thermodata Europe (SGTE) [19], the calculation of the quantities of interest can easily be performed using the application software Thermo-Calc [20]. We then reformulate our calculated thermodynamic functions reported in [14] and compare them with the database built in CALPHAD.

The form suggested for Gibbs free energies of the unary phases is as follows:

$$G_i^{\Phi}(T) \equiv {}^{0}G_i^{\Phi}(T) - H_i^{\mathrm{SER}} = a + bT + cT\ln(T) + dT^2 + eT^3 + fT^{-1} + \cdots \quad (1)$$

The left-hand side of Eq. (1) is the Gibbs free energy of the element $i$ in the structure $\Phi$, $G_i^{\Phi}(T)$, relative to a standard element reference (SER) state of the element $i$ in its stable state at 298.15 K and 1 bar, $H_i^{\mathrm{SER}}$. The coefficients $a, b, \ldots, f$ that enter Eq. (1) for the pure elements that are used by SGTE [20] are taken from Dinsdale's compilation [21]. In the following and for comparison purposes we adopted the SGTE description of Cu and Fe in the various phases considered, namely fcc, bcc, and liquid.

For a binary phase $\Phi$, the Gibbs free energy is written as

$$G^{\Phi}(\{x_i\}, T) = {}^{\mathrm{ref}}G^{\Phi}(\{x_i\}, T) + {}^{\mathrm{id}}G^{\Phi}_{\mathrm{mix}}(\{x_i\}, T) + {}^{\mathrm{xs}}G^{\Phi}_{\mathrm{mix}}(\{x_i\}, T), \quad (2)$$

where $x_i$ is the molar fraction of species $i$ in the $\Phi$ phase, and the terms on the right-hand side are, respectively, the concentration weighted average molar Gibbs energy associated with the pure elements, the molar Gibbs ideal mixing energy, and the excess Gibbs energy due to non-ideal contributions. In the general case of a multi-component solution in a particular phase $\Phi$, the excess Gibbs energy of mixing is expressed by a Redlich–Kister expansion [22], and the terms on the right-hand side of Eq. (2), are expressed as follows:

$$\begin{aligned} {}^{\mathrm{ref}}G^{\Phi}(\{x_i\}, T) &= \sum_i x_i G_i^{\Phi}(T), \\ {}^{\mathrm{id}}G^{\Phi}_{\mathrm{mix}}(\{x_i\}, T) &= RT\sum_i x_i \ln(x_i), \\ {}^{\mathrm{xs}}G^{\Phi}_{\mathrm{mix}}(\{x_i\}, T) &= \sum_i \sum_{j>i} x_i x_j \sum_{p=0}^{n} {}^{p}L^{\Phi}_{i,j}(T)(x_i - x_j)^p, \end{aligned} \quad (3)$$

where ${}^{p}L^{\Phi}_{i,j}(T)$ is the $p$th-order binary interaction parameter between species $i$ and $j$ relative to phase $\Phi$, usually expressed as polynomials in temperature and pressure.

In the present study the Fe–Cu binary system was assessed as follows. A one-sublattice model has been considered to describe the liquid, the fcc-A1 and the bcc-A2 solid solution phases with expressions for the molar Gibbs energy given by Eq. (3). The excess Gibbs energy is expressed by a three (1,2)-term Redlich–Kister expansion for the liquid (bcc, fcc) phase, and a linear function of temperature for each of the Redlich–Kister terms. For the description of the alloy, the data, reported in Appendix A, are from the SSOL database [23] that is used in combination with the Thermo-Calc software [20], while those in Appendix B correspond to our computational results reported in detail in Ref. [14]. Note that although a more recent CALPHAD optimization has been performed for Fe–Cu alloys [24], the conclusions reported in this paper remain basically unchanged. The resulting phase diagram using the CALPHAD database that we use for comparison purposes, is shown in Fig. 1.

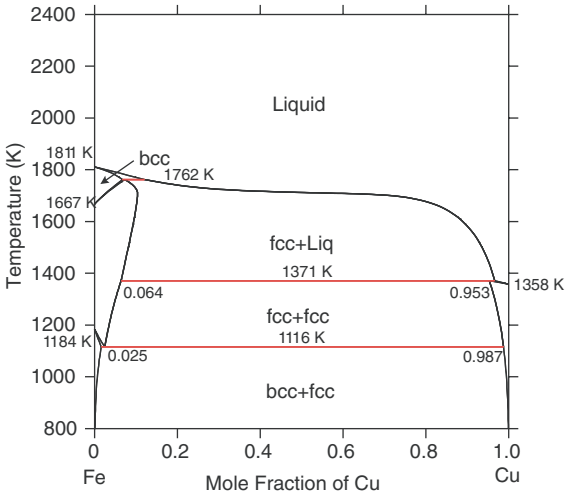


Fig. 1. Calculated Fe–Cu phase diagram obtained from the application of Thermo-Calc to the CALPHAD data summarized in Appendix A.

## 3. CALPHAD parametrization of the FS numerical results

We calculated the free energy per particle, $f(T)$, at a given temperature $T$ through a thermodynamic integration between the state of interest and a reference state at temperature $T_0$ with known free energy $f(T_0)$ (obtained using the switching Hamiltonian method), according to the Gibbs–Duhem equation (for details on the procedure, see Ref. [14]):

$$f(T) = f(T_0)\frac{T}{T_0} - T\int_{T_0}^{T} \frac{h(\tau)}{\tau^2}\,\mathrm{d}\tau, \quad (4)$$

where $h(\tau)$ is the enthalpy per particle. The enthalpy (obtained from a MD run) is described by a second-order polynomial in $T$, allowing an analytic integration in Eq. (4):

$$-T\int_{T_0}^{T} \frac{h^{\phi}(c,\tau)}{\tau^2}\,\mathrm{d}\tau = a_c^{\phi} - b_c^{\phi}T\ln(T) - c_c^{\phi}T^2 + d_c^{\phi}T. \quad (5)$$

This procedure leads to the following general equation for the free energy of each phase $\phi$, at composition $x_{\mathrm{Cu}}$:

$$g^{\phi}(x_{\mathrm{Cu}}, T) = a^{\phi}(x_{\mathrm{Cu}}) - b^{\phi}(x_{\mathrm{Cu}})T\ln(T) - c^{\phi}(x_{\mathrm{Cu}})T^2 + d_G^{\phi}(x_{\mathrm{Cu}})T - Ts_{\mathrm{conf}}(x_{\mathrm{Cu}}). \quad (6)$$

In our original description of the free energy at a given composition and temperature, $g(x_{\mathrm{Cu}}, T)$ c.f. Ref. [14],

we used second order polynomial fits for the dependence of the coefficients on the composition $x_{Cu}$. We first choose $x_{Cu} = 0$ and 1 in Eq. (6) to obtain $g^{\phi}_{Fe}(T)$ and $g^{\phi}_{Cu}(T)$, respectively. Now, we translate these expressions into the CALPHAD formalism that uses the Redlich–Kister power series [21] for the free energy in excess of the ideal solution:

$$g^{\phi}(x_{Cu}, T) = {}^{ref}g^{\phi}(x_{Cu}, T) + {}^{id}g_{mix}(x_{Cu}, T) + {}^{xs}g^{\phi}_{mix}(x_{Cu}, T), \tag{7}$$

where

$${}^{ref}g^{\phi}(x_{Cu}, T) = x_{Cu}g^{\phi}_{Cu}(T) + (1 - x_{Cu})g^{\phi}_{Fe}(T), \tag{8}$$

$${}^{id}g_{mix}(x_{Cu}, T) = RT[x_{Cu}\ln(x_{Cu}) + (1 - x_{Cu})\ln(1 - x_{Cu})] \tag{9}$$

and

$${}^{xs}g^{\phi}_{mix}(x_{Cu}, T) = x_{Cu}(1 - x_{Cu})\sum_{p} {}^{p}L^{\phi}_{Cu,Fe}(T)(2x_{Cu} - 1)^{p}, \tag{10}$$

where the coefficients ${}^{p}L^{\phi}$ are functions of temperature for each phase $\phi$ (pressure is always zero in this work). If the summation in Eq. (10) extends only to $p = 0$, we are left with what is called in text books the quasi-chemical approximation, namely, ${}^{xs}g^{\phi}_{mix}(x_{Cu}, T) = x_{Cu}(1 - x_{Cu})\Omega$. The polynomial expression in Eq. (10) thus describes how the parameter $\Omega$ depends on the composition, having the quasi-chemical approximation as a particular case.

By equating Eqs. (6) and (7), and keeping in mind that in the fitting procedure reported in [14] the coefficients of Eq. (6) are second-order polynomials in $x_{Cu}$, we find that it is equivalent to retain only the $p = 0$ term in the series and that this ${}^{0}L^{\phi}_{Cu,Fe}(T)$ is given by

$${}^{0}L^{\phi}_{Cu,Fe}(T) = -a^{\phi}_{2} - d^{\phi}_{2}T + b^{\phi}_{2}T\ln(T) + c^{\phi}_{2}T^{2}, \tag{11}$$

where the sub-index 2 in the coefficients refer to the quadratic terms in the $T$ expansion of the coefficients $a$, $b$, $c$, and $d$ in Eq. (6), see Appendix B. We realize now that by keeping only a second-order polynomial to describe the concentration dependence of the coefficients of the free energy in Ref. [14], we in fact choose to have symmetric excess free energies of each phase in the solid solution [17].

With Eqs. (6) and (11) a database in the CALPHAD format can be created, see appendix, and the Thermo-Calc software can be conveniently used to accurately calculate the phase diagram. The results are shown in Fig. 2, together with an inset showing an enlarged view of the high-temperature, Fe-rich part with the peritectic invariant line. Within a few degrees Kelvin, it is quite comparable to the one reported in Ref. [14] that resulted from a simple but laborious common tangent construction. The advantage of using software such as Thermo-Calc is that we can readily compare the free energies, enthalpies and entropies of the model Fe–Cu alloy under consideration with the standard CALPHAD database mentioned in the previous section.

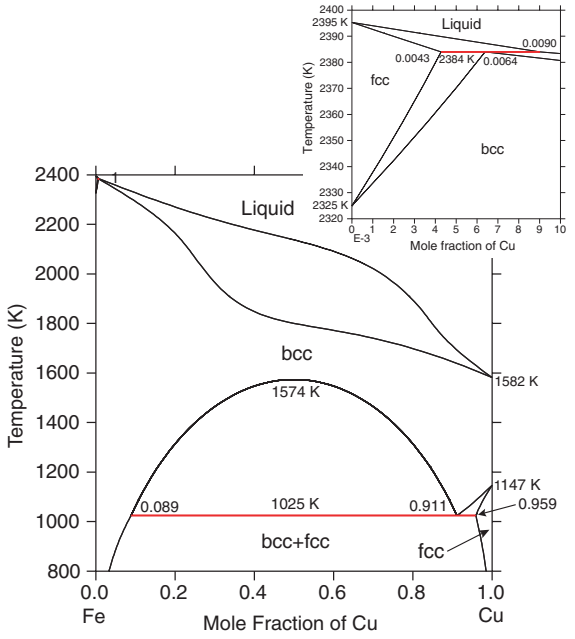


Fig. 2. Predicted Fe–Cu phase diagram obtained from the application of the Thermo-Calc software to the results of FS simulations summarized in Appendix B. The inset shows an enlarged view of the high-temperature, Fe-rich part with the peritectic invariant line.

## 4. Thermodynamic analysis

Let us now analyze these results in order of importance from the point of view of their impact on MD simulations of microstructure evolution of Fe–Cu dilute solutions. In this sense, the bcc phase of Cu appearing at 1150 K, together with the bcc–fcc transition of Fe are the most striking features.

To understand which contribution to the free energies is primarily responsible for these phase transitions, we show in Figs. 3 and 4 the enthalpies and entropies of the FS-Cu and Fe, respectively, together with the reference database. To define a common zero of the enthalpy scale for comparison purposes, the values of the enthalpy of fcc Cu (331 962 J/mol; cf. Fig. 3, top panel), and bcc Fe (408 901 J/mol; cf. Fig. 4, top panel), both at $T = 298.15$ K, have been subtracted to all (three phases) enthalpy curves. The agreement between both curves for fcc Cu, Fig. 3 (upper panel) is very satisfactory at all temperatures below melting, indicating the adequacy of the FS formalism to describe thermody-

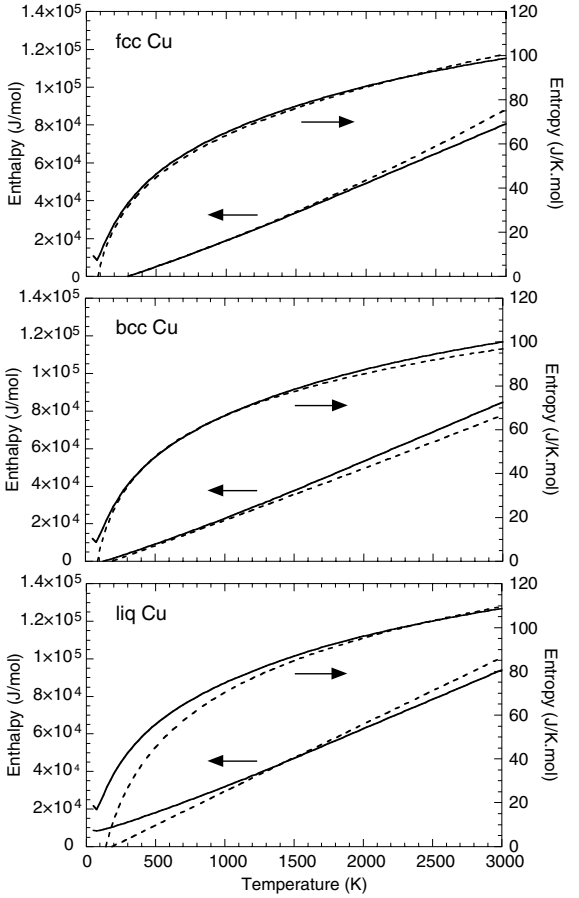


Fig. 3. Enthalpy (in J/mol) and entropy (in J/K mol) for the fcc, bcc, and liquid phases of pure Cu as functions of temperature (in K). The solid (dashed) lines refer to the CALPHAD (FS) results. The enthalpy of the fcc ground state at 298.15 K is taken as zero of energy.

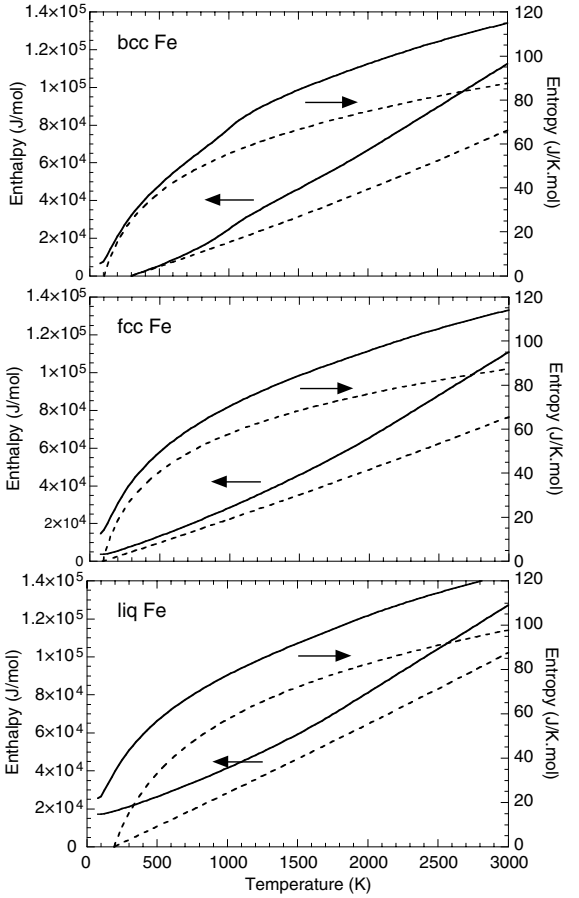


Fig. 4. Same as caption of Fig. 3 but for pure Fe. The enthalpy of the bcc ground state at 298.15 K is taken as zero of energy.

namic properties of pure Cu. It is important to acknowledge that a departure at high temperatures between the curves is to be expected due to contributions that are neglected either in the FS–MD model, such as electronic heat capacity, electronic temperature contribution to changes in the potential energy surface, or in the simulation, such as the contribution from the equilibrium vacancy concentration.

The same comparison for the Cu bcc phase, Fig. 3 (middle panel) shows a discrepancy, namely, a more stable bcc phase for the FS-Cu than for the assessed data in the entire temperature range, but more noticeable above 1000 K. This signals already one possible contribution to the erroneous enhanced stability of the FS-Cu bcc phase. The last comparison, the FS-Cu enthalpy for the liquid phase is compared to the assessed data in Fig. 3 (lower panel). Although a significant difference appears in its temperature dependence, it fortuitously happens that in the region around the experimental $T_m$ both curves have similar values, indicating that, if the bcc phase of Cu would not appear as a stable phase, the fcc crystal would melt quite at the right $T$, provided the entropy contribution is correct.

A similar comparison for the Cu vibrational entropy in all three phases is shown in the same Fig. 3. The agreement for the fcc phase is quite satisfactory over the entire temperature range, and the same can be said for the bcc phase up to the melting temperatures. The liquid entropy, instead, is too small in the region of interest, and this causes an increase in the melting temperature.

With these comparisons, we can already state that the reason for the presence of a high temperature bcc phase in Cu is the too small bcc enthalpy, or equivalently the too small bcc–fcc energy difference. Entropy in turn, which is related to vibrational frequencies, i.e. second derivatives of the energy, are quite correct for both fcc and bcc phases of Cu, at least in the temperature range of interest, but is too small for the liquid phase, which

implies a too high melting temperature for the fcc and bcc phases. Finally, the fcc phase of FS-Cu is quite correctly described in terms of its enthalpy and entropy.

The fcc–bcc energy difference at zero temperature is a parameter usually considered in the development of classic potentials, but in the case of this potential it has only been checked that the bcc energy at 0 K lies above the fcc value (c.f. Ref. [3]). The FS result gives +2275 J/mol, while the CALPHAD value is +4011 J/mol.

It is interesting to see what the melting temperature of the fcc Cu would be if the bcc phase is suspended from the thermodynamic analysis by increasing its enthalpy. This happens to be 1499 K, 10.5% higher than the experimental value.

Focusing now on the Fe behavior, Fig. 4 show the enthalpy and entropy for the bcc, fcc, and liquid phases. The discrepancies are notorious in all three phases. The reasons for this are to be found in the magnetic and electronic contributions [25]. At the Curie temperature of Fe, $T_C = 1033$ K, an anomaly is observed in the enthalpy as well as in the entropy of the CALPHAD bcc phase, which is, of course, absent in the classic prediction. The non-magnetic fcc phase is nonetheless also poorly described. It is interesting to note that the CALPHAD database shows that the enthalpy of both bcc and fcc phases are quite similar above 1500 K, while the FS predictions are both not only well below the CALPHAD values but also quite different. In Ref. [25] a quantitative estimation of the lattice, electronic and magnetic contributions to the specific heat is performed, in which the lattice component is modeled with a Debye model, the electronic component is modeled with a linear term and the magnetic one is obtained as the difference between the experimental value and the two previous contributions. In this way the authors find expressions for the specific heat below and above the Curie temperature showing the cusp at the ferromagnetic–paramagnetic transition.

Entropies of the bcc, fcc and liquid phases are also shown in Fig. 4. Here again, the discrepancies are very important. Above 1500 K, all three bcc, fcc and liquid FS entropies are $\sim 2k_B$/at. below the CALPHAD values.

From these enthalpies and entropies, the free energies of the different phases can be drawn. The usual way to show these curves is as free energy difference with respect to the stable phase of each material. Fig. 5 shows the free energy differences for FS and CALPHAD Cu (upper panel) and Fe (lower panel). Arrows indicate the phase transitions between the relevant phases: the first arrow from the left in the upper panel indicates the fcc to bcc transition of FS Cu at 1147 K, the second shows the real fcc melting. The third arrow shows melting of the FS-fcc Cu, while the last one shows a curious re-entrance of the fcc phase as the stable one above ~2700 K, if the liquid phase is disregarded. This is against the observation that the bcc phase is usually

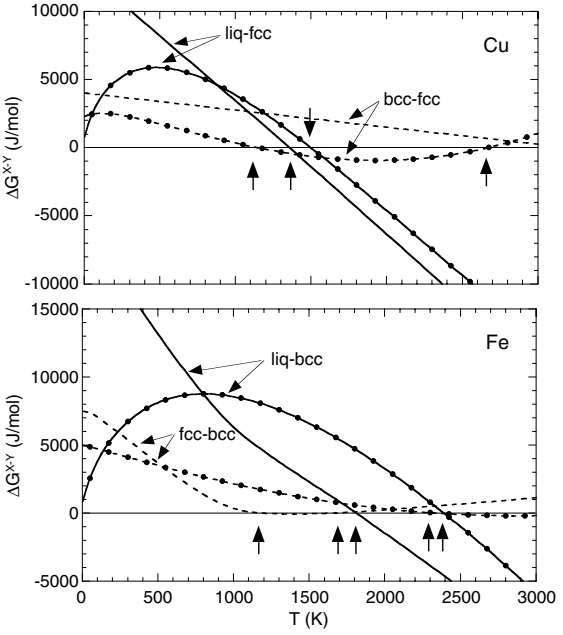


Fig. 5. Structural molar Gibbs energy difference (in J/mol), $\Delta G^{X-Y}$, as a function of temperature (in K) for Cu (top panel) and Fe (bottom panel). $X$ = liq and $Y$ = fcc (solid line), $X$ = bcc and $Y$ = fcc (dashed line) for Cu, and $X$ = liq and $Y$ = bcc (solid line), $X$ = fcc and $Y$ = bcc (dashed line) for Fe. The curves without (with) dots refer to the CALPHAD (FS) results. The arrows locate the zeros of $\Delta G^{X-Y}$ which indicate phase transitions.

the stable phase at high T for metals due to the smaller entropy (or equivalently, smaller Einstein frequency) associated to a smaller number of neighbors [26].

For Fe, the arrows in Fig. 5 (lower panel) indicate (from left to right) the bcc–fcc transition, the re-entrance of the fcc phase, the melting of fcc Fe, the bcc to fcc FS transition, and the melting of the FS fcc Fe.

The discrepancies among these curves is so severe that, in the case of Cu, it is hard to establish any degree of reliability in predictions like the relative stability of bcc versus fcc precipitates of Cu in Fe. However, in qualitative terms, it can be said that the FS and CALPHAD free energy difference curves for Cu run approximately parallel in the temperature ranges where each one is relevant, suggesting that the temperature dependence of these functions is correctly captured by the FS model. This gives hope that it may be possible to improve the free energy description of FS Cu by an appropriate fit to these thermodynamic functions.

For Fe in turn, the situation is more complex in the sense that a significant difference exists between the temperature dependence of the fcc–bcc curves obtained from FS and CALPHAD, as shown in Fig. 5. All three FS phases of Fe have a rather weak T-dependence, reflecting the absence of contribution from the electronic

degrees of freedom and magnetism in the FS formalism. Although these differences are huge, we may speculate that the free energy *differences*, as those reported in Fig. 5, are the relevant thermodynamic functions determining equilibrium phases and driving forces in non-equilibrium processes. A difference between the CALPHAD and FS fcc–bcc free energies can probably not be solved in a simple way within the FS framework. However a description of Fe much closer to reality may be obtained if the free-energy difference between the liquid and bcc phases can be substantially reduced, given the fact that its temperature dependence is quite correct but its absolute value is greater by a significant amount.

So far we discussed the pure elements. Now we analyze the behavior of the alloy at 1100 K. Fig. 6(a) shows the excess enthalpy of mixing according to CALPHAD and FS, for the three phases under consideration. The first evidence that comes out of this figure is that the FS, despite having been adjusted to the experimental heats of solution of a single impurity (i.e., to the derivatives of these curves at $x_{Cu} = 0$ and 1) fails to describe the strength of the repulsion in concentrated alloys in all three phases. There is more than a factor of two between the CALPHAD and the FS values. The second observation is that the FS curves are symmetric with respect to equi-atomic composition, $x_{Cu} = 0.5$, while the real alloys show a slight asymmetry, mainly in the fcc phase.

Fig. 6(b) shows the excess entropy of mixing (vibrational) that is the temperature-dependent contribution to the excess Gibbs energy of mixing given by Eq. (3) (third equation) for CALPHAD or Eq. (10) for FS. While the CALPHAD results show positive contributions, asymmetric for the solid phases and symmetric for the liquid phase, the FS results predict negative, symmetric ones. The influence of this wrong prediction of the vibrational entropy on the final value of free energy is not so dramatic if we consider that mixing entropy gives a contribution that is 3–5 times larger than this vibrational one, in such a way that the final excess entropy (vibrational + configurational) is positive for all phases in both datasets, with FS approximately one half the CALPHAD values.

Fig. 6(c) displays the Gibbs free energies for all three phases at 1100 K. It is clearly seen through a common tangent construction that the impact of these enthalpy–entropy differences results in much higher FS solubility limits for both terminal phases.

Contrary to FS-Cu, FS-Fe presents so severe departures from real Fe, originated in the limitation of the classic approximation to account for electronic and magnetic contributions, that it is difficult to say how much better a Fe potential can be devised within this empirical framework. However, if we focus on free-energy differences between the phases, to address problems

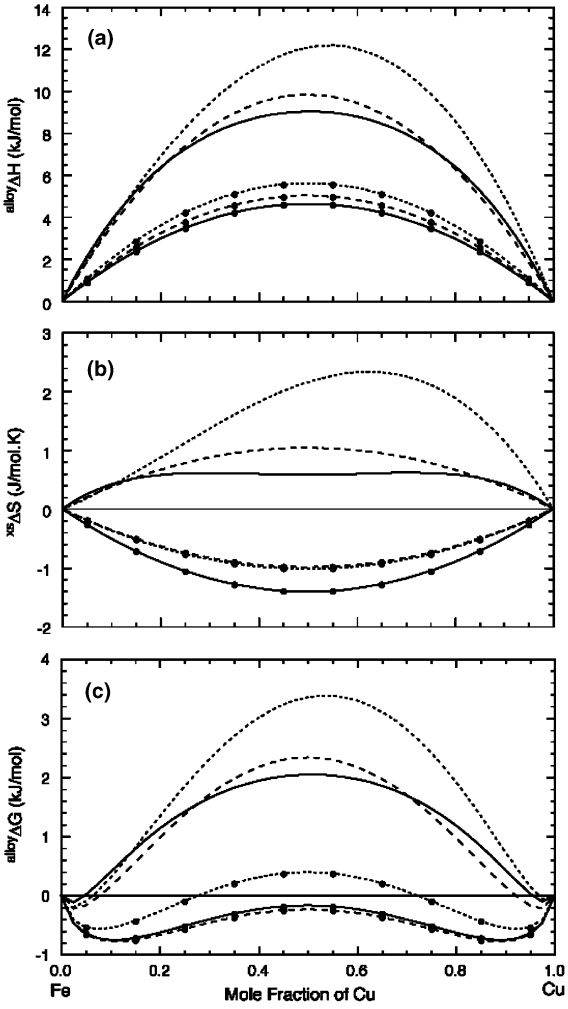


Fig. 6. Excess molar enthalpy $^{alloy}\Delta H$ (in J/mol), vibrational entropy $^{alloy}\Delta S$ (in J/K mol), molar Gibbs energy $^{alloy}\Delta G$ (in J/mol) for Fe–Cu alloys as functions of the Cu composition at $T = 1100$ K. The solid (dashed, dotted) line corresponds to the liquid (bcc, fcc) phase of the alloy. The curves without (with) dots refer to the CALPHAD (FS) results.

of phase equilibrium and kinetics of phase transformations, it seems possible to decrease the enthalpy of FS-liquid Fe to lower its melting point, in which case the spurious fcc phase of Fe would not appear in the equilibrium diagram. This would already represent a substantial improvement.

The analysis presented so far shows that besides the fcc phase of Cu, all other phases present in the Fe–Cu system have serious discrepancies with the thermodynamic data of the real system. This fact does not necessarily reflect unsolvable limitations of the empirical approach to describe real materials, but certainly sheds light on the unquestionable necessity of incorporating thermodynamic data during the initial stage of potential

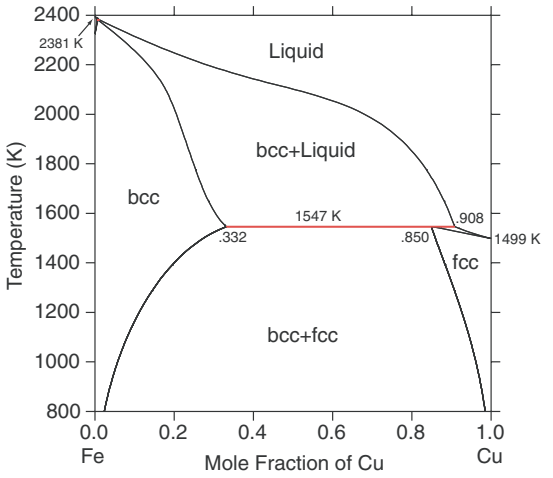


Fig. 7. Predicted Fe–Cu phase diagram obtained from the application of the Thermo-Calc software to the modified results of FS simulations summarized in the appendix. An additional +4017 J/mol was added to the FS description of the Gibbs energy of the bcc phase of pure Cu (see text).

development, so that the main features of real multicomponent alloys are captured. We can speculate that some of the problems reported here may eventually be solved. For instance, it seems possible to increase the enthalpy of the bcc Cu to remove it from the phase diagram. Also, a small change in enthalpy and/or entropy of fcc and liquid Cu could help to adjust the melting point of pure Cu. As an example, we present in Fig. 7 the phase diagram of Fe–Cu obtained from FS results after adding an energy of +4011 J/mol to the bcc phase of Cu, so that the energy difference between fcc and bcc Cu is identical to the energy difference in the CALPHAD approach (note that this is just a shift into the enthalpy predicted by the potential, not a redesign of the potential, which is not the objective of the present work). With a new Cu potential that would introduce this modification into the energetics, the phase diagram presented in Fig. 7 is probably the best that can be expected from empirical potentials for Fe–Cu alloys in the sense of phases present. It remains to decrease the solubility limit by increasing the enthalpy of mixing, what would probably require a different description of the hetero-atomic interactions.

## 5. Conclusions

We conclude from this study that alloys in the framework of empirical potentials require a different treatment of the hetero-atomic interactions if the concentrated cases are to be correctly described. Both Fe–Cu as well as the case we studied previously, Au–Ni, show that adjusting the heat of solution of a single impurity is not enough to describe the complex behavior of concentrated systems. This problem, we believe, can be addressed by further modifications to the empirical formalism to incorporate concentration dependent interactions that will reproduce the magnitude of excess enthalpy of mixing, as well as the asymmetry around equi-atomic composition. Additionally, a careful check of the energetics of all possible phases of the pure elements appears also as a critical issue to correctly predict the equilibrium phases, avoiding the appearance of spurious.

## Acknowledgments

Work performed under the auspices of the US Department of Energy by the University of California Lawrence Livermore National Laboratory under contract No. W-7405-ENG-48, and CONICET, Argentina, PIP-0664/98. Discussions with L. Kaufman are gratefully acknowledged. We thank L. Malerba for careful reading of the manuscript.

## Appendix

Thermodynamic parameters (energy in J/mol, temperature $T$ in K) that describe the Fe–Cu system. Parameters not indicated here are set to zero. Notations are explained in Section 2 of the main text. Note that within CALPHAD an additional magnetic contribution to the Gibbs energy, that is not reported here, has to be included for pure Fe in the bcc and fcc phases (cf. Ref. [22]). If no temperature range is specified this implies that the data are applicable at any temperature.

### Appendix A. Within CALPHAD (from Ref. [22])

- Liquid: (Cu, Fe)

$$\begin{aligned} G^{\mathrm{liq}}_{\mathrm{Cu}} &= +12\,964.84 - 9.510243T - 5.83932\times 10^{-21}T^{7} \\ &\quad + G^{\mathrm{fcc}}_{\mathrm{Cu}}, \quad 298.15\ \mathrm{K} < T < 1358.02\ \mathrm{K} \\ &= +13\,495.4 - 9.920463T - 3.64643\times 10^{29}T^{-9} \\ &\quad + G^{\mathrm{fcc}}_{\mathrm{Cu}}, \quad 1358.02\ \mathrm{K} < T < 3200\ \mathrm{K}, \end{aligned}$$

$$\begin{aligned} G^{\mathrm{liq}}_{\mathrm{Fe}} &= +1225.7 + 124.134T - 23.5143T\ln(T) \\ &\quad - .00439752T^{7} - 5.8927\mathrm{E}-08T^{3} + 77\,359T^{-1} \\ &\quad + G^{\mathrm{fcc}}_{\mathrm{Cu}}, \quad 298.15\ \mathrm{K} < T < 1811\ \mathrm{K} \\ &= -25\,383.581 + 299.31255T - 46T\ln(T) \\ &\quad + 2.2960310^{+31}T^{-9} + G^{\mathrm{bcc}}_{\mathrm{Fe}}, \\ &\quad 1811\ \mathrm{K} < T < 6000\ \mathrm{K}, \end{aligned}$$

$${}^{0}L^{\mathrm{liq}}_{\mathrm{Cu,Fe}} = +36\,087.987 - 2.3296885T,$$

$${}^{1}L^{\mathrm{liq}}_{\mathrm{Cu,Fe}} = +324.52964 - .032700618T,$$

$${}^{2}L^{\mathrm{liq}}_{\mathrm{Cu,Fe}} = +10\,355.386 - 3.6029763T.$$

- bcc: (Cu, Fe)

$$G^{\mathrm{bcc}}_{\mathrm{Cu}} = +4017 - 1.255T + G^{\mathrm{fcc}}_{\mathrm{Cu}}, \quad 298.15\ \mathrm{K} < T < 3200\ \mathrm{K},$$

$$\begin{aligned} G^{\mathrm{bcc}}_{\mathrm{Fe}} &= +1225.7 + 124.134T - 23.5143T\ln(T) \\ &\quad - .00439752T^2 - 5.8927\times 10^{-8}T^3 \\ &\quad + 77\,359T^{-1}, \quad 298.15\ \mathrm{K} < T < 1811\ \mathrm{K} \\ &= -25\,383.581 + 299.31255T - 46T\ln(T) \\ &\quad + 2.29603\times 10^{31}T^{-9}, \quad 1811\ \mathrm{K} < T < 6000\ \mathrm{K}, \end{aligned}$$

$${}^{0}L^{\mathrm{bcc}}_{\mathrm{Cu,Fe}} = +39\,257.976 - 4.1498304T.$$

- fcc: (Cu, Fe)

$$\begin{aligned} G^{\mathrm{fcc}}_{\mathrm{Cu}} &= -7770.458 + 130.485403T - 24.112392T\ln(T) \\ &\quad - .00265684T^2 + 1.29223\times 10^{-7}T^3 \\ &\quad + 52\,478T^{-1}, \quad 298.15\ \mathrm{K} < T < 1358.02\ \mathrm{K} \\ &= -13\,542.33 + 183.804197T - 31.38T\ln(T) \\ &\quad + 3.64643\times 10^{29}T^{-9}, \quad 1358.02\ \mathrm{K} < T < 3200\ \mathrm{K}, \end{aligned}$$

$$\begin{aligned} G^{\mathrm{fcc}}_{\mathrm{Fe}} &= -1462.4 + 8.282T - 1.15T\ln(T) + 6.4\mathrm{E}-04T^2 \\ &\quad + G^{\mathrm{fcc}}_{\mathrm{Cu}}, \quad 298.15\ \mathrm{K} < T < 1811\ \mathrm{K} \\ &= -27\,098.266 + 300.25256T - 46T\ln(T) \\ &\quad + 2.78854\times 10^{31}T^{-9} + G^{\mathrm{fcc}}_{\mathrm{Cu}}, \\ &\quad 1811\ \mathrm{K} < T < 6000\ \mathrm{K}, \end{aligned}$$

$${}^{0}L^{\mathrm{fcc}}_{\mathrm{Cu,Fe}} = +48\,232.565 - 8.6095425T,$$

$${}^{1}L^{\mathrm{fcc}}_{\mathrm{Cu,Fe}} = +8861.8816 - 5.2897513T.$$

## Appendix B. From an FS description of alloy thermodynamics

- Liquid: (Cu, Fe)

$$\begin{aligned} G^{\mathrm{liq}}_{\mathrm{Cu}} &= -6754.975494 + 215.8308996T \\ &\quad + 0.0001299078\,30T^2 - 36.2183687T\ln(T), \end{aligned}$$

$$\begin{aligned} G^{\mathrm{liq}}_{\mathrm{Fe}} &= -6541.346078 + 214.4482650T \\ &\quad - 0.0006646487\,53T^2 - 34.2281661T\ln(T), \end{aligned}$$

$$\begin{aligned} {}^{0}L^{\mathrm{liq}}_{\mathrm{Cu,Fe}} &= +10\,514.0049616 + 71.6509610T \\ &\quad + 0.00121146964T^2 - 8.58265838T\ln(T). \end{aligned}$$

- bcc: (Cu, Fe)

$$\begin{aligned} G^{\mathrm{bcc}}_{\mathrm{Cu}} &= -5002.892143 + 143.8084700T \\ &\quad - 0.000367416086T^2 - 26.4848335T\ln(T), \end{aligned}$$

$$\begin{aligned} G^{\mathrm{bcc}}_{\mathrm{Fe}} &= -7072.015320 + 131.4515955T \\ &\quad - 0.0016300229\,40T^2 - 23.2336643T\ln(T), \end{aligned}$$

$$\begin{aligned} {}^{0}L^{\mathrm{bcc}}_{\mathrm{Cu,Fe}} &= +22\,519.6729195 - 31.0132753T \\ &\quad - 0.00256978993T^2 + 5.07753979T\ln(T). \end{aligned}$$

- fcc: (Cu, Fe)

$$\begin{aligned} G^{\mathrm{fcc}}_{\mathrm{Cu}} &= -7217.140161 + 126.5781221T \\ &\quad - 0.00281924306T^2 - 23.3658491T\ln(T), \end{aligned}$$

$$\begin{aligned} G^{\mathrm{fcc}}_{\mathrm{Fe}} &= -2093.372978 + 130.4481482T \\ &\quad - 0.00086810734T^2 - 23.6089921T\ln(T), \end{aligned}$$

$$\begin{aligned} {}^{0}L^{\mathrm{fcc}}_{\mathrm{Cu,Fe}} &= +26\,403.2069170 - 17.0991278T \\ &\quad + 0.001174515\,76T^2 + 2.32491019T\ln(T). \end{aligned}$$

## References


[1] W.J. Phythian, A.J.E. Foreman, C.A. English, J.T. Buswell, M.G. Hetherington, K. Roberts, S. Pizzini, in: 15th International Symposium Effects of Radiation on Materials, 19–21 June 1990, Nashville, TN, ASTM STP, vol. 1125, American Society for Testing and Materials, Philadelphia, 1992, p. 131.

[2] W.J. Phythian, C.A. English, J. Nucl. Mater. 205 (1993) 162.

[3] G.J. Ackland, G. Tichy, V. Vitek, M.W. Finnis, Philos. Mag. A 56 (1987) 735.

[4] Yu.N. Osetsky, A.G. Mikhin, A. Serra, Philos. Mag. A 72 (1995) 361.

[5] Yu.N. Osetsky, A. Serra. Philos. Mag. A 73 (1996) 249.

[6] Yu.N. Osetsky, A. Serra, Philos. Mag. A 75 (1997) 1097.

[7] G.R. Odette, B.D. Wirth, J. Nucl. Mater. 251 (1997) 157.

[8] B.D. Wirth, G.R. Odette, Mater. Res. Soc. Symp. Proc. 540 (1999) 637.

[9] C. Domain, C.S. Becquart, J.C. Van Duysen, Mater. Res. Soc. Symp. Proc. 540 (1999) 643.

[10] J.J. Blackstock, G.J. Ackland, Philos. Mag. A 81 (2001) 2127.

[11] G.J. Ackland, D.J. Bacon, A.F. Calder, T. Harry, Philos. Mag. A 75 (1997) 713.

[12] M.W. Finnis, J.E. Sinclair, Philos. Mag. A 50 (1984) 45.

[13] F. Ercolessi, M. Parrinello, E. Tosatti, Philos. Mag. A 58 (1988) 213.

[14] E.M. Lopasso, M. Caro, A. Caro, P.E.A. Turchi, Phys. Rev. B 68 (2003) 214.

[15] T.B. Massalski (Ed.), Binary Alloy Phase Diagrams, vols. 1–3, ASM International, Materials Park, OH, 1990.

[16] L. Kaufman, H. Bernstein, Computer Calculation of Phase Diagrams with Special Reference to Refractory Metals, Academic Press, New York, 1970.
[17] N. Saunders, A.P. Miodownik, CALPHAD, Calculation of Phase Diagrams: a Comprehensive Guide, Pergamon, New York, 1998.
[18] P.J. Spencer (Guest Ed.), MRS Bulletin, 24 (4) (1999) 18 (Materials Research Society, Warrendale, PA).
[19] I. Ansara, B. Sundman, in: P.S. Glaeser (Ed.), Computer Handling and Dissemination of Data, Elsevier, Amsterdam, 1987.
[20] B. Sundman, B. Jansson, J.-O. Andersson, CALPHAD 9 (1985) 153.
[21] A. Dinsdale, CALPHAD 15 (1991) 317.
[22] O. Redlich, A. Kister, Ind. Eng. Chem. 40 (1948) 345.
[23] A. Jansson, Report D 73, Metallografi, KTH, 1986.
[24] M.A. Turchanin, P.G. Agraval, I.V. Nikolaenko, J. Phase Equil. 24 (3) (2003) 307.
[25] Y.-Y. Chuang, R. Schmid, T.A. Chang, Metall. Trans. A 16 (1985) 153.
[26] J. Friedel, J. Phys. 35 (1974) L-59.